The Importance of Atmospheric Dynamics in the Northern Hemisphere Wintertime Climate Response to Changes in the Earth's Orbit

ALEX HALL

Department of Atmospheric Sciences, University of California, Los Angeles, Los Angeles, California

AMY CLEMENT

Rosenstiel School of Marine and Atmospheric Science, University of Miami, Miami, Florida

DAVID W. J. THOMPSON

Department of Atmospheric Science, Colorado State University, Fort Collins, Colorado

ANTHONY BROCCOLI

Department of Environmental Sciences, Rutgers–The State University of New Jersey, New Brunswick, New Jersey

CHARLES JACKSON

Institute for Geophysics, The John A. and Katherine G. Jackson School of Geosciences, University of Texas at Austin, Austin, Texas

(Manuscript received 27 January 2004, in final form 23 September 2004)

ABSTRACT

Milankovitch proposed that variations in the earth's orbit cause climate variability through a local thermodynamic response to changes in insolation. This hypothesis is tested by examining variability in an atmospheric general circulation model coupled to an ocean mixed layer model subjected to the orbital forcing of the past 165 000 yr. During Northern Hemisphere summer, the model's response conforms to Milankovitch's hypothesis, with high (low) insolation generating warm (cold) temperatures throughout the hemisphere. However, during Northern Hemisphere winter, the climate variations stemming from orbital forcing cannot be solely understood as a local thermodynamic response to radiation anomalies. Instead, orbital forcing perturbs the atmospheric circulation in a pattern bearing a striking resemblance to the northern annular mode, the primary mode of simulated and observed unforced atmospheric variability. The hypothesized reason for this similarity is that the circulation response to orbital forcing reflects the same dynamics generating unforced variability. These circulation anomalies are in turn responsible for significant fluctuations in other climate variables: Most of the simulated orbital signatures in wintertime surface air temperature over midlatitude continents are directly traceable not to local radiative forcing, but to orbital excitation of the northern annular mode. This has paleoclimate implications: during the point of the model integration corresponding to the last interglacial (Eemian) period, the orbital excitation of this mode generates a 1°–2°C warm surface air temperature anomaly over Europe, providing an explanation for the warm anomaly of comparable magnitude implied by the paleoclimate proxy record. The results imply that interpretations of the paleoclimate record must account for changes in surface temperature driven not only by changes in insolation, but also by perturbations in atmospheric dynamics.

1. Introduction

Much of the internal variability of the present-day climate stems from well-known modes of climate variability. These modes are products of dynamical processes within the atmosphere–ocean system. Prominent among them are the El Niño–Southern Oscillation (ENSO) phenomenon in the Tropics (Philander 1990), and the annular modes in the extratropics of the Northern (e.g., Hurrell 1995, Thompson and Wallace 2000; Hurrell et al. 2003) and Southern (e.g., Kidson 1988; Karoly 1990; Hartmann and Lo 1998; Thompson and Wallace 2000) Hemispheres. Like ENSO, the northern annular mode (NAM, also known as the North Atlantic Oscillation and Arctic Oscillation) is linked with significant variability in temperature and other climate variables because of its association with atmospheric

Corresponding author address: Alex Hall, Dept. of Atmospheric Sciences, University of California, Los Angeles, Los Angeles, CA 90095.
E-mail: alexhall@atmos.ucla.edu

circulation anomalies (e.g., Hurrell et al. 2003). It would therefore alter surface climate if it were perturbed. The dynamical response of ENSO to orbital forcing has been proposed as an important component of paleoclimate variability (Clement et al. 1999). However, the extratropical paleoclimate has not been viewed in terms of known modes of variability, and attention has commonly focused instead on the direct thermodynamic response to orbital forcing, particularly on how variations in boreal summer insolation can lead to an ice age (Hays et al. 1976; Imbrie et al. 1984). In this study, we demonstrate that the dynamics of NAM are crucial to understanding the Northern Hemisphere (NH) extratropical wintertime response of a climate model to pure orbital forcing.

2. Experimental design

The model we use to study this issue is an atmospheric general circulation model on a global domain coupled to mixed layer ocean model consisting of an isothermal 50-m-depth slab. The model has a resolution of approximately 4.5° latitude × 7.5° longitude (see Fig. 2a for a view of the model's NH distribution of oceans and continents). There are nine vertical levels, with the top level coinciding roughly with a pressure of 25 hPa. As is standard practice when such a model configuration is employed, seasonal variations in deep ocean heat transport are included as a prescribed flux at the bottom of the ocean mixed layer. These heat fluxes are chosen to maintain present-day sea surface temperatures (SSTs) when the present-day orbital configuration is imposed. Sea ice dynamics and thermodynamics are included. A simple land surface model is employed, where surface temperatures are determined by heat balance assuming no storage of heat within the land. Soil moisture is predicted using a 15-cm-depth bucket model formulation.

The variations in insolation associated with changes in the earth's orbit of the past 165 000 yr, taken from Berger (1992), are imposed on the model in a continuous fashion. We remind the reader briefly of the properties of this solar forcing. It results from variations in the obliquity of the earth's spin axis relative to the plane of the earth's orbit about the sun, precession of the earth's spin axis, and fluctuations in the eccentricity of the earth's orbit. Obliquity varies on a time scale of about 40 000 yr. This changes the geographical distribution of insolation on both a seasonal- and annual-mean basis. When obliquity is high, the summertime extratropics receive more sunshine, while less is received elsewhere. The anomaly in the summertime extratropics is much larger than the anomaly elsewhere. On an annual-mean basis the Tropics receive less sunshine when obliquity is high, while the high latitudes receive more. The earth's spin axis completes one precessional cycle in about 20 000 yr. This cycle affects the time of year the earth comes closest to the sun (perihelion). The entire earth receives more sunshine at perihelion, so that the precessional forcing is in phase globally for any given time of year; however, the anomaly is largest in the lower the zenith angle. For example, if perihelion coincides with NH summer solstice, the insolation anomaly is larger in the NH. Unlike obliquity, precession does little to alter the geographical distribution of annual-mean insolation. Variations in eccentricity, occurring on approximately 100 000-yr time scales, also generate very little annual-mean signal. Their main effect is to modulate the strength of the precessional forcing.

The pace of the orbital variations of the past 165 000 yr is accelerated by a factor of 30 in the simulation, so that the actual integration only lasts 5500 yr. The acceleration, which makes the experiment practical given limited computational resources, does not compromise our ability to diagnose the simulated response to orbital forcing, since the model equilibrates to the forcing within 10 model years. Even with the orbital variations taking place at the accelerated pace, this equilibration time is still approximately two orders of magnitude shorter than the time scale of the forcing's shortest periodicity. Since the experiment's goal is to isolate the effect of orbital forcing on climate variability, these are the only boundary conditions that change over the course of the integration. Carbon dioxide and ozone, the only greenhouse gases in the model other than water vapor, are fixed to present-day levels. The present-day configuration of continental ice sheets is prescribed. The experiment therefore isolates the simulated response of the atmosphere–ocean system to orbital forcing in the absence of variations stemming from the historical growth and decay of the North American and Scandinavian ice sheets. More detailed descriptions of the model and experimental design are provided in Jackson and Broccoli (2003).

3. Analysis techniques

In all raw model time series, both variability generated internally by the model and fluctuations stemming from orbital forcing are noticeable. A typical example of this is seen in Fig. 1a, which shows the simulated time series of sea level pressure (SLP) at a grid point near the Azores in the central North Atlantic. Here pronounced variations in SLP on orbital times scales are visible, as are higher-frequency fluctuations clearly unrelated to orbital forcing and therefore generated by the model's internal dynamics. To separate the orbital and internal variability, the raw time series are projected onto obliquity and precession basis functions using a least squares fitting procedure. The time series of deviations of a given climatic quantity from its mean value of the 165 000-yr simulation $X(t)$, is expressed as

$$X(t) = A_o\Phi'(t) + A_p e(t)\cos[\lambda(t) - \varphi_p] + R(t), \quad (1)$$

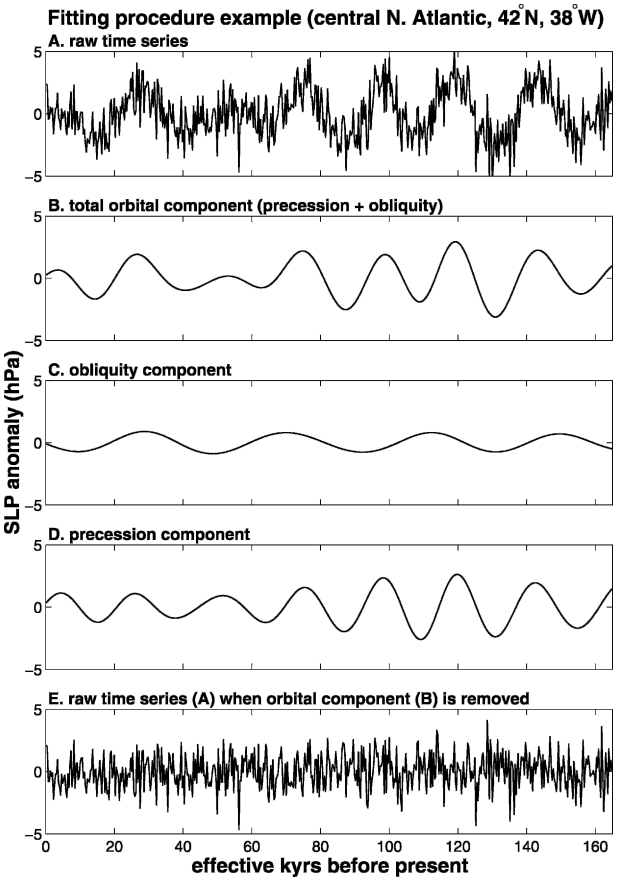

FIG. 1. An example of the least squares fitting procedure used to separate raw model time series into orbital and internal variability components. (a) The raw model time series of SLP at a grid point near the Azores in the central North Atlantic (42°N, 38°W). Orbital periodicities as well as internal variability are clearly visible. (b) The variability in (a) that can be linearly related to orbital forcing, given by the sum of the variability that can be linearly related to (c) obliquity forcing and to (d) precessional forcing. (e) What remains when the orbital variability of (b) is subtracted from the raw model time series in (a). This is clearly mostly internally generated variability. The abscissa of each panel spans 165 000 yr (30 times the actual 5500-yr length of the model integration) to reflect the forcing acceleration technique described in section 2. Decadal means of the 5500-yr-long model time series were used so that only 550 data points are plotted in each panel.

where t is time, Φ' is the deviation of obliquity from its 165 000-yr mean, e is the eccentricity, and λ is the longitude of perihelion. The fitting procedure determines A_o, the amplitude of the response that can be linearly related to obliquity forcing, as well as A_p, the amplitude and φ_p, the phase of the response that can be linearly related to precessional forcing. The residual $R(t)$ contains the remainder of the variability.

Lags in the atmosphere–ocean system could make a climate variable at any given time of year more sensitive to orbital insolation anomalies at an earlier time of year. For this reason we allow climate variables to have a phase as well as an amplitude relationship with the orbital forcing in Eq. (1). The phase relationship is treated differently in the precession and obliquity cases. Precessional forcing has a phase relationship with the annual cycle that varies continuously through the ~20 000-yr precessional cycle. Therefore we allow the precession-related climate response to be anywhere from 0° to 360° out of phase with the precessional forcing. A concrete instance of this, which we discuss later in this article, is the simulated response of SST to precessional forcing. Because of the ocean's thermal inertia, SST at any given time of year is generally most sensitive to solar forcing two to three months earlier. For example, the precession-related SST variations in January tend to reach their maximum value over much of the ocean when perihelion occurs in October, and so are in phase with the precessional variation of insolation in October. This information can be captured with an amplitude (A_p) and a phase (φ_p).

Obliquity forcing, unlike its precession counterpart, does not have a continuously varying phase relationship with the annual cycle. This is because obliquity-induced insolation anomalies throughout the calendar year are either in phase or out of phase with variations in the tilt of the earth's axis. An obliquity-related climate anomaly at any particular time of year may result from an instantaneous response to a simultaneous insolation anomaly or may instead stem from a sensitivity to obliquity forcing during another season. Either way, it will be either in phase or out of phase with obliquity variations. This information can be captured simply by allowing A_o to be either positive or negative. Our method of extracting the simulated response to obliquity forcing is only appropriate for our atmosphere–mixed layer ocean modeling framework, where the model equilibrates quickly to changes in orbital configuration. If our atmospheric model were coupled instead to a fully dynamical ocean model, response time lags of thousands of years could occur in the deep ocean, and we would need to allow for a continuously varying phase relationship with obliquity to capture this.

Figures 1b–e illustrate how the least squares fitting procedure works for the Azores SLP time series in Fig. 1a. Figure 1c shows $A_o\Phi'(t)$, the variability in the time series that can be linearly related to obliquity forcing. Figure 1d shows $A_p e(t) \cos[\lambda(t) - \varphi_p]$, the variability that can be linearly related to precessional forcing. The obliquity and precession variations can be combined to give a time series of the total variability that can be linearly related to orbital forcing, which we denote as "orbital" variability (Fig. 1b) throughout this paper. A comparison of Figs. 1a,b reveals that the least squares fitting procedure works reasonably well; there is a clear correspondence, both in amplitude and phase, between the orbital variability captured by the least squares fitting procedure and the orbital variations seen in the raw time series.

In principle, $R(t)$, the variability remaining when the orbital variability is removed from raw model time series includes three types of fluctuations: 1) internal variability, 2) nonlinear response to orbital forcing, and 3) direct effects of the 100 000-yr variations in eccentricity. In practice, however, in most variables at most locations it is clear from visual inspection of $R(t)$ that internal variability overwhelmingly dominates the other two types of fluctuations (e.g., Fig. 1e). We therefore denote the residual remaining when orbital variability is removed from raw model time series as "internal" variability throughout this paper.

4. Annular mode response

The model's NH extratropical response to orbital forcing and its main modes of internal variability in this region can be summarized by an empirical orthogonal function (EOF) analysis of orbital and internal SLP variability (Fig. 2). We show results from both summer [June–July–August (JJA)] and winter [December–January–February (DJF)] seasons to highlight the dramatic difference in the simulated response to orbital forcing between these two seasons.

In summer, the signatures of local heating predominate in the primary pattern of the seasonal-mean SLP response to orbital forcing (Fig. 2a). This pattern consists of anomalously low SLP over continents, and high SLP over oceans. The time series associated with it (black curve, Fig. 2b) is nearly perfectly correlated with a time series representing June NH extratropical orbital forcing (insolation anomalies at 40°N, orange curve, Fig. 2b). When the NH extratropics receive more summer insolation, the land areas warm more than the ocean because of smaller evaporative damping and effective heat capacity over land. This causes a monsoon-like shift of atmospheric mass from the land to ocean.

If the main mode of orbital seasonal-mean SLP variations during winter could also be understood as a local thermodynamic response to orbital forcing, Fig. 2e would be similar to Fig. 2a with smaller amplitudes owing to the smaller size of the DJF insolation anomalies, and the time series associated with it would also be in phase with the forcing. Instead, Fig. 2e shows high SLP concentrated in two lobes over the midlatitude oceans and low SLP over the Arctic, and the associated time series is significantly out of phase with the time series representing December NH extratropical forcing (cf. orange and black curves in Fig. 2f). These features are difficult to explain as a local thermodynamic response to orbital forcing.

The primary mode of orbital DJF SLP variability, shown in Fig. 2e, bears a striking resemblance to the primary mode of internal wintertime SLP variability, shown in Fig. 2g. With high pressure in two lobes associated with the NH Atlantic and Pacific storm tracks, and low pressure over the Pole, this is the model's northern annular mode (NAM). The pattern is very similar to the real atmosphere's NAM (Thompson and Wallace 2000), despite the atmospheric model's coarse resolution. The NAM is hypothesized to dominate wintertime variability in both observations and models because of a positive feedback between midlatitude westerlies and transient eddies in the NH storm tracks (Lorenz and Hartmann 2003). During the positive phase of the NAM, the extratropical eddies flux anomalously large amounts of westerly momentum across ~45°N (Limpasuvan and Hartmann 2000), giving rise to out-of-phase anomalies in the zonal wind between 30°–35° and 55°–60°N. The anomalies in the zonal wind, in turn, organize eddy activity such that the anomalies in the zonal flow are reinforced (Lorenz and Hartmann 2003; Robinson 2000).

The relationship between zonal wind and the NAM is mirrored in the simulation, as seen in the projection of the internal zonal-mean, zonal wind variability onto the primary mode of internal SLP variability (Fig. 3b) When orbital zonal winds are projected onto the primary mode of orbital SLP variability (Fig. 3a), westerly anomalies centered near 55°–60°N and easterly anomalies centered near 30°–35°N also result. Thus, both the horizontal and vertical structures of the primary mode of orbital variability closely resemble those of the NAM. This suggests the same eddy–mean flow interactions governing the primary mode of internal wintertime circulation variability are also at play in selecting the primary mode of orbital wintertime circulation variability. Though they reflect the same fundamental phenomenon, we simplify the following discussion by denoting the mode portrayed in Fig. 2e as the "orbital NAM," and the mode portrayed in Fig. 2g as the "internal NAM." The NAM pattern does not dominate internal SLP variability in summer (Fig. 2c), consistent with the dearth of eddy activity at this time of year.

A comparison of the SLP values shown in Figs. 2e, g indicates that the magnitudes of the SLP anomalies associated with the orbital NAM are comparable to those associated with the internal NAM. This is also suggested by visual inspection of the internal and orbital components of the central North Atlantic SLP time series (shown in Figs. 1b and 1e, respectively). This grid point is located in the North Atlantic lobe of the NAM. The internal and orbital fluctuations here, both of which are associated in large part with the NAM-like modes of variability in Figs. 2e,g, are comparable in magnitude.

5. The meridional SST gradient and the orbital NAM

Robinson (2000) and Kushnir et al. (2002) argue that changes in the meridional surface temperature gradient in midlatitudes can induce changes in the NAM via the relationship between lower-tropospheric baroclinicity

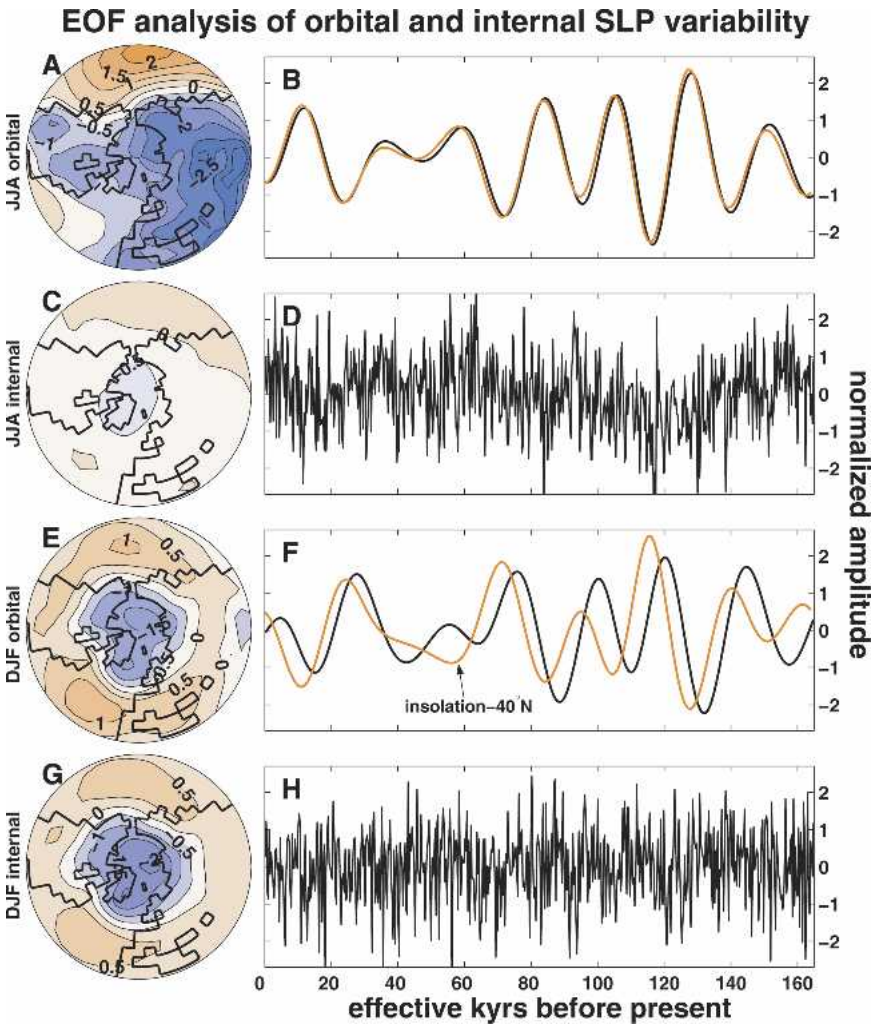

FIG. 2. The patterns of (a), (c), (e), (g) the first EOFs and (b), (d), (f), (g) the associated time series (black lines) for orbital and internal variability components of simulated SLP poleward of 26.7°N. (a), (b) JJA orbital variability. The pattern accounts for 96% of the orbital variance. (c), (d) JJA internal variability. This pattern accounts for 36% of the internal variance. (e), (f) DJF orbital variability. This pattern accounts for 80% of the variance. (g), (h) DJF internal variability. This pattern accounts for 61% of the variance. When the EOF analysis is performed separately on the obliquity and precession components of the JJA (DJF) orbital variability, the patterns closely resemble each other and those of (a) [(e)], so that (a) [(e)] summarizes the main mode of SLP variability for both types of orbital forcings. JJA and DJF decadal means of the 5500-yr-long model time series were used for this analysis, so that only 550 data points are plotted in (b), (d), (f), (h). Also shown with orange lines are the incoming solar radiation anomalies at 40°N resulting from variations in the earth's orbit, normalized by their std dev, for (b) Jun and (f) Dec. The phasing of these curves is representative of the phasing of the orbital forcing over the entire NH extratropics because both their obliquity and precessional components are in phase with the orbital forcing elsewhere in the NH extratropics, as implied by the discussion of the character of the orbital forcing given in section 2. The abscissas of (b), (d), (f), (h) span 165 000 yr (30 times the actual 5500-yr length of the model integration) to reflect the forcing acceleration technique described in section 2.

and the convergence of the eddy momentum flux in the upper troposphere. They theorize that along a latitude of the enhanced meridional surface temperature gradient, there is increased generation of baroclinic eddies in the lower troposphere and thus increased convergence of the momentum flux in the upper troposphere as the eddies radiate away from their source latitude. The combined effects of the anomalous heat and momentum fluxes by the eddies give rise to equivalent barotropic westerly anomalies throughout the depth of the

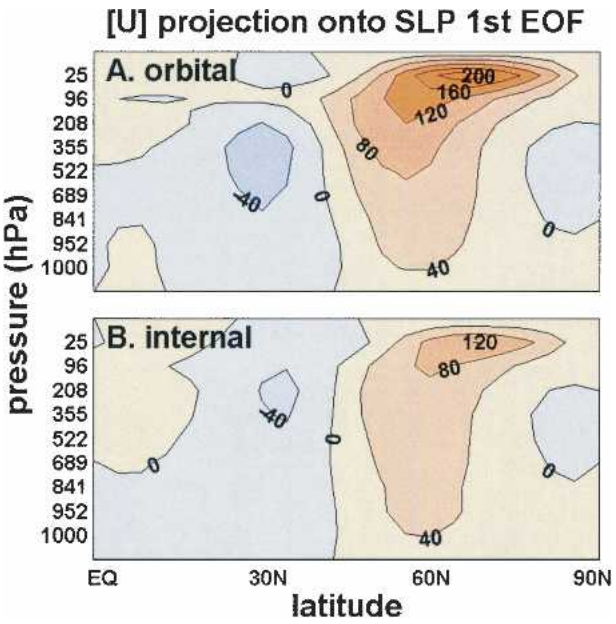

FIG. 3. The vertical structure of the DJF zonal-mean zonal wind ($[U]$) anomalies accompanying the primary modes of SLP orbital and internal variability. Units in all panels are cm s^{-1}. (a) Regression of the orbital component of $[U]$ onto the EOF time series shown in Fig. 2f (black curve). (b) Regression of the internal variability component of $[U]$ onto the EOF time series shown in Fig. 2h.

troposphere. Here we draw on this mechanism to argue that orbitally induced variations in the wintertime extratropical meridional temperature gradient across the main axis of the westerly NAM anomalies near 55°N are very likely to be key to understanding why the model response to orbital forcing during NH winter is dominated by a pattern nearly identical to the NAM. For this reason we explain in this section how orbital variations in this temperature gradient arise in the simulation. We analyze the fluctuations stemming from obliquity and precessional forcing separately, since the mechanisms whereby the two types of forcing generate these fluctuations are different.

We focus first on obliquity. Figure 4a shows a Hovmöller diagram of the obliquity component of wintertime zonal-mean SST variability. A clear out-of-phase relationship is seen between SST poleward and equatorward of about 45°N. When obliquity is high, DJF SSTs fall below the mean in the Tropics, and rise above the mean in high latitudes. This pattern reveals that the wintertime SST response to obliquity forcing is controlled by the annual-mean insolation anomaly. When obliquity is high, the high latitudes receive significantly more insolation in the summertime, while the Tropics receive less. Though in winter the entire hemisphere receives less sunshine when obliquity is high, the summertime forcing is much larger than that of winter, so that the annual-mean forcing is dominated by the summertime signal. Hovmöller plots of zonal-mean SST for each of the other seasons (not shown), reveal a nearly identical pattern to that in Fig. 4a, confirming that the mixed layer ocean has enough memory of the large summertime forcing in the nonsummer seasons that the SST response follows the summertime forcing throughout the year. The dashed line in Fig. 4b summarizes this relationship between obliquity and the extratropical meridional SST gradient: When obliquity is high (low), the gradient is weakened (strengthened).

Figure 5a shows a Hovmöller diagram of the precessional component of NH zonal-mean SST variability. The strongest signals are seen equatorward of about 50°N, with the anomalies becoming larger about 80 000–140 000 yr before present, when the eccentricity of the earth's orbit was the greatest of the past 165 000 yr. These signals reach their maximum value when perihelion occurs in mid-fall, and can be understood as a lagged thermodynamic response to precessional forcing. Just as SSTs reach their maximum values two to three months after the summer solstice in the context of the present-day seasonal cycle, these anomalies reach their maximum values in our simulation when perihelion occurs about two to three months prior to the midpoint of the winter season. This explains why the precessional component of the October-mean insolation anomaly at 40°N (Fig. 5b, orange line) is nearly perfectly in phase with the precessional component of subtropical wintertime SST variability. The relative strength of the precessional signal equatorward of 50°N (owing largely to the fact that the magnitude of the precessional forcing itself increases equatorward) means that these latitudes dominate precessional variations in the extratropical meridional SST gradient. A comparison of Fig. 5a to the dashed line in Fig. 5b shows that the precessional variations in the extratropical meridional SST gradient are closely in phase with precessional variations in subtropical SST.

The causal relationship between the meridional SST gradient and the orbital NAM pattern is suggested by an examination of Figs. 4b and 5b; both the obliquity and precession components of the meridional SST gradient are nearly perfectly in phase with their respective components of the orbital NAM. The direction of causality between the SST gradient and the NAM is somewhat ambiguous because the NAM also gives rise to a meridional surface temperature gradient via compressional heating and cooling in the zonally symmetric vertical motion associated with it; however, the SST anomalies seen in Figs. 4a and 5a are very consistent with a direct thermodynamic response to orbital forcing. Moreover the wintertime SST response to orbital forcing behaves very similarly to the SST response in other seasons (not shown), when dynamical processes are much weaker and the direct thermodynamic response is sure to dominate. The high likelihood that the SST anomalies in Figs. 4a and 5a mainly reflect a direct thermodynamic response to orbital forcing implies that fluctuations in the extratropical meridional SST gradi-

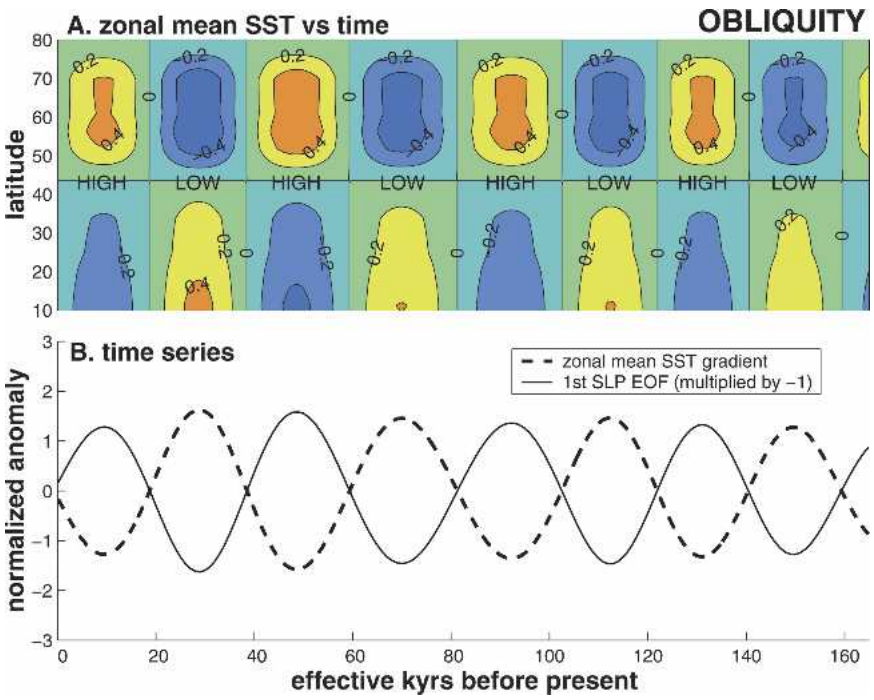

FIG. 4. Summary of NH wintertime relationship between zonal-mean SST and the primary mode of SLP variability for anomalies related to obliquity variations. (a) Hovmöller diagram of the obliquity component of zonal-mean DJF SST (°C) in the NH. Also noted on this panel are times when obliquity is anomalously high and low. (b) Normalized time series of the obliquity component of the NH extratropical zonal-mean DJF SST gradient (dashed line), defined as the difference in zonal-mean DJF SST between 38°and 74°N. Shown as a solid line in (b) is the obliquity component of the time series associated with the first EOF of orbital DJF SLP variability (Fig. 2f). This time series has been multiplied by −1 to avoid visual interference with the zonal-mean SST gradient time series.

ent are forcing orbital NAM variability, rather than the other way around.

6. Impacts of orbital NAM variability

Significant surface air temperature (SAT) variability is associated with the NAM, as indicated by the projection of internal SAT anomalies onto the internal NAM time series (Fig. 6c). The stronger surface westerlies implied by the SLP pattern in Fig. 2g advect warm marine air over cold continents, and cold continental air over warm oceans. This creates a zonally asymmetric SAT pattern, with warm SATs over mid- to high-latitude continents, and cold SATs over mid- to high-latitude oceans. The anomalies are particularly large over northern Europe, Canada, the Greenland Sea, and the northern North Pacific. This is very similar to the SAT pattern associated with the positive phase of the real atmosphere's NAM (e.g., Hurrell 1995, Thompson and Wallace 2000). These authors also demonstrated that the SAT anomalies associated with the observed NAM result from advection of warm and cold air masses by the NAM's anomalous circulation, as described above.

A somewhat similar pattern to Fig. 6c emerges when orbital SATs are projected onto the orbital NAM (Fig. 6a), with warm temperatures over northern Europe and Canada, and cold temperatures over the Greenland Sea and northern North Pacific. However, this pattern is difficult to interpret definitively because it contains SAT anomalies from two sources: 1) those generated by the circulation anomalies associated with the orbital NAM, as in the unforced case, and 2) those related to the SST anomalies responsible for exciting the orbital NAM (Figs. 4 and 5). The latter result from the direct thermodynamic response to orbital forcing, as described in section 4. Since they are related to the mechanism forcing the orbital NAM, they are highly correlated with the orbital NAM index. However, they obviously cannot be interpreted as an impact of the orbital NAM.

To clarify this issue, we removed the zonal-mean variability from the orbital SAT time series and reprojected the zonally asymmetric orbital SAT variability onto the orbital NAM time series (Fig. 6b). This allow us to focus more on the SAT impact of the orbital NAM because SAT anomalies resulting from variability in the surface westerlies across the zonally asymmet-

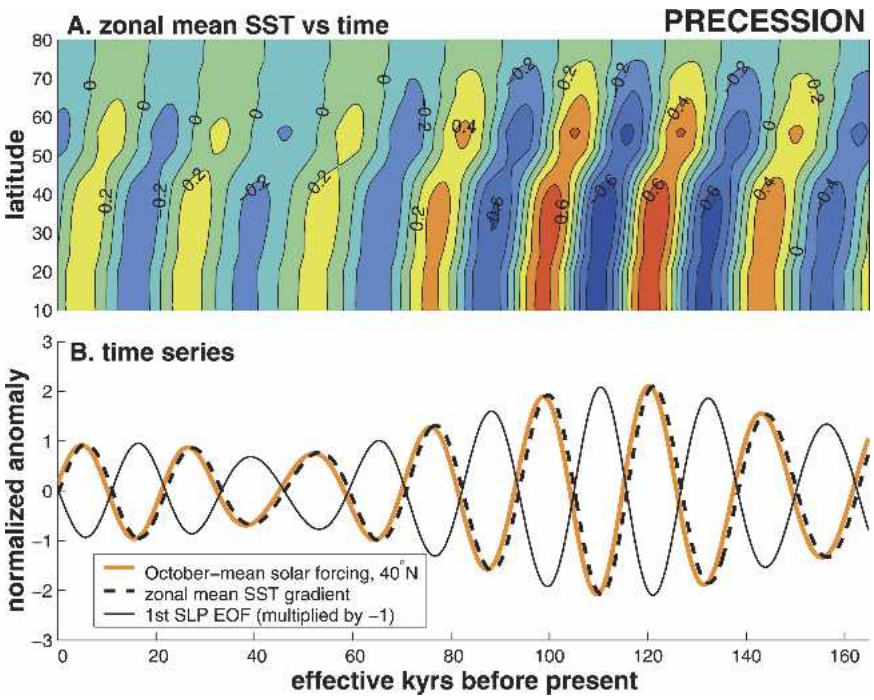

FIG. 5. As in Fig. 4, except for anomalies related to the precession of the earth's spin axis. (b) Solid orange line is the normalized time series of the precessional component of Oct-mean orbital insolation anomalies at 40°N.

ric NH land–ocean configuration are more strongly reflected in the zonally asymmetric component of orbital SAT variability, while SAT anomalies resulting directly from the zonally symmetric orbital forcing are more strongly reflected in the zonally symmetric component. The overwhelming similarity between Figs. 6b and 6c suggests that this decomposition worked: Since the pattern in Fig. 6c can be thought of as an impact of the internal NAM, the fact that the pattern in Fig. 6b is nearly identical to it suggests the zonally asymmetric component of orbital SAT variability can be understood as an impact of the orbital NAM.

Over North America and Eurasia poleward of about 45°N, the zonally symmetric SAT pattern of Fig. 6b accounts for most of the total orbital SAT variability seen in Fig. 6a. In these regions, simulated continental wintertime SAT variations traceable to orbital forcing are therefore determined mainly by the orbital forcing

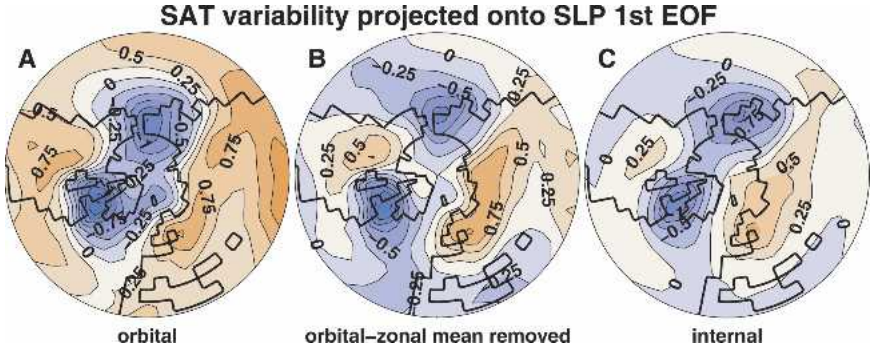

FIG. 6. (a) Regression of orbital DJF SAT (°C) variability onto the time series associated with the first EOF of orbital DJF SLP variability (Fig. 2f, black curve). (b) Regression of the zonally asymmetric component of orbital DJF SAT variability onto the time series associated with the first EOF of orbital DJF SLP variability. Zonally asymmetric SAT variations were calculated by first removing the zonal-mean SAT variation. (c) Regression of internal DJF SAT variability onto the time series associated with the first EOF of internal DJF SLP variability (Fig. 2h).

of the atmospheric circulation, rather than a local response to radiative forcing. We return to this point when we discuss the paleoclimate implications of our study in section 7.

7. Rules of thumb

Lacking the observed variation in ice volume over the past 165 000 yr, our simulation likely differs in significant ways from the actual climate variations during this period, particularly at times when the ice sheet distribution differed significantly from the present. However, our idealized experiment gives useful rules of thumb that can be used to interpret the actual paleoclimate record and understand past controls on the NAM:

1) *Difference between the summer and winter response of the NH climate.* During summertime, the circulation response can be understand in terms of a simple local thermodynamic response to orbital forcing; a positive insolation anomaly warms the continents more than the oceans, which leads to low SLP over continents and high SLP over the oceans. On the other hand, in wintertime, the NH response to orbital forcing includes not only a passive thermodynamic response, but also a dynamic response that resembles the dominant mode of internal atmospheric variability. The direct wintertime thermodynamic response to orbital forcing gives rise to variations in the NH extratropical meridional SST gradient. Consistent with the mechanisms outlined in Robinson (2000) and Kushnir et al. (2002), the changes in the midlatitude surface temperature gradient are associated with changes in the tropospheric zonal flow that project onto the signature of the NAM. The dominance of the NAM in internal wintertime variability, and its weakness in summer, can be traced to the relative strength of synoptic-scale eddy activity in winter.
2) *Importance of the extratropical meridional SST gradient during winter.* The tight relationship between orbital variations in this quantity and the wintertime circulation suggests it may be particularly useful for understanding past NH wintertime climate variability. Paleoclimate proxies of anomalies in this gradient, whether they arise from orbital forcing or for other reasons, may provide information about past variations in the wintertime circulation and climate.
3) *Seasonal lags between forcing and response*. Examining the climate response to continuously varying orbital forcing forces one to confront seasonal lags between forcing and response. Because of the thermal inertia of the ocean, the phasing of the primary mode of the orbital wintertime circulation variability is controlled by insolation anomalies in other seasons: The obliquity component phasing is controlled by annual-mean obliquity forcing, which is dominated by the summertime obliquity signal, while the phasing of the precessional component is controlled by the fall precessional signal. This information would have been overlooked if we had approached this problem by simply taking snapshots of the simulated climate response to orbital forcing at different moments in the past, as is often done in paleoclimate modeling. The design of our experiment and the results we obtained from it also underscores the possibility that any seasonal climate signal revealed in a paleoclimate proxy is not necessarily related to insolation anomalies in that same season, as is often assumed to be the case.

8. Implications

The variability simulated in our model may correspond to actual climate variations during periods of the past 165 000 yr when the ice sheet distribution resembled that of the present day. This condition is met during the Holocene period, extending approximately 11 000 yr before present. An examination of the time series of the orbital NAM (black curve, Fig. 2f) reveals the orbital forcing did not cause large NAM-like fluctuations. This apparently weak response during the Holocene period arises largely because of destructive interference between the obliquity and precessional components of the time series (cf. the solid black curves in Figs. 4b and 5b). The insolation in mid-fall due to precession was greater than normal during the Holocene period, reaching a maximum when perihelion occurred in October approximately 6000 yr ago. This strengthened the extratropical wintertime meridional SST gradient. Obliquity, on the other hand, was relatively high during this period, weakening the extratropical wintertime meridional SST gradient. This partially counteracted the precessional forcing and made for only relatively small perturbations to the wintertime circulation: We created a combined orbital and internal NAM index based on the raw model time series over the past 11 000 yr by taking the difference in DJF zonal-mean pressure between 38°N and the North Pole. In this time series (not shown), the orbital signals are barely visible, being dominated by the internal variability. We therefore predict small perturbations to the NAM due to orbital forcing during the Holocene period compared to levels of variability generated internally by the atmosphere.

The ice sheet distribution also resembled that of the present-day during the last interglacial, or Eemian period, which lasted from approximately 130 000 to 110 000 yr before present. In contrast to the Holocene period, the orbital NAM reached its maximum value of the entire model time series at about this time (Fig. 2f, black curve), peaking about 120 000 yr before present. This is mainly because perihelion occurred in the NH in the fall then, and high eccentricity at this time amplified

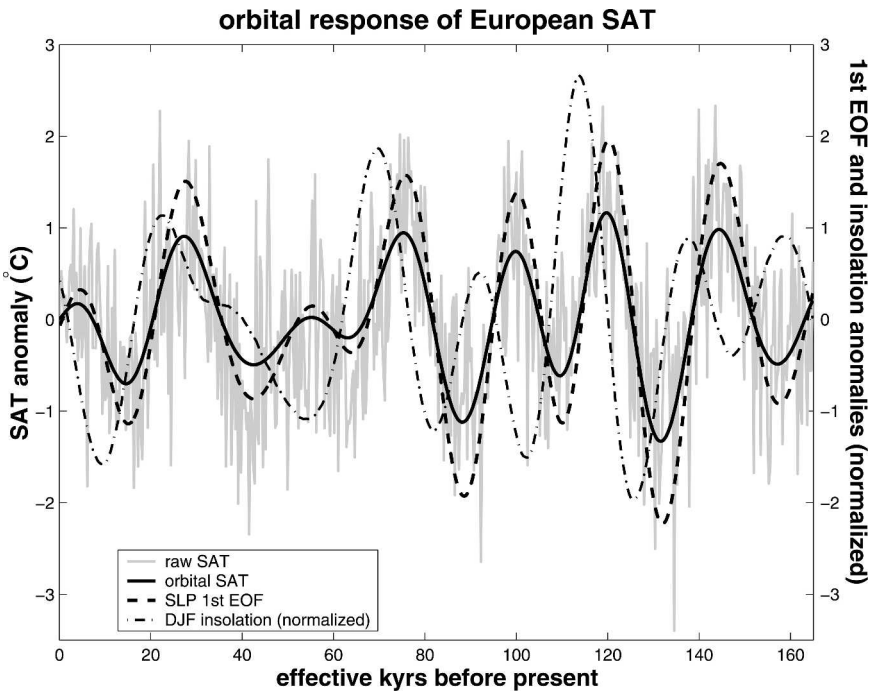

FIG. 7. Time series of: 1) orbital DJF SAT (°C) averaged over the model's European continent, which includes all land areas from 36° to 77°N, and from 4°W to 56°E. 2) The DJF incoming insolation due to Milankovitch forcing averaged over these same latitudes. This time series has been normalized by its standard deviation. 3) The primary mode of orbital SLP variability (same as the black curve in Fig. 2f). The raw 30-yr-mean DJF SAT anomaly time series averaged over the model's European continent is also shown in light gray.

the precessional forcing (Fig. 5b). (Figure 4 shows that obliquity was near average at this time, so that obliquity forcing contributed little to the Eemian maximum in the orbital NAM.) This may explain why paleoclimate proxy records indicate winters in Europe during the mid-Eemian period were significantly warmer than the present day (Zagwijn 1996; Aalbersberg and Litt 1998, Klotz et al. 2003). A high NAM index at this time would have increased advection of warm maritime air over the European continent, increasing temperatures there, as in Fig. 6b.

In fact, a time series of simulated orbital SAT averaged over the European continent reaches its maximum of the entire simulation at the midpoint of the Eemian period, approximately 120 000 yr ago (Fig. 7, solid black curve). The SAT in this continental area might be expected to equilibrate quickly to direct orbital forcing and would therefore be in phase with DJF insolation anomalies if SAT simply responded thermodynamically to orbital forcing. This is the case in summer: JJA insolation anomalies over Europe are nearly perfectly in phase with JJA SATs (not shown). However, it is clear from Fig. 7 that DJF insolation anomalies averaged over the latitudes of Europe are not in phase with SAT. Instead, there is a nearly perfect in-phase relationship between European SAT and the orbital NAM. The ~1.2°C simulated warming over Europe 120 000 yr ago relative to the present can account for a significant fraction of the roughly 2°C wintertime warming inferred from various paleoclimate proxy data (Zagwijn 1996; Klotz et al. 2003). This comparison must not be taken too literally, of course, as the model result represents a continent-wide average, while the proxy data are representative of local conditions and feedbacks completely unresolved by this coarse resolution model. Still, the simulated orbital SAT signal is large enough to suggest that wintertime European temperature fluctuations during the Eemian period were controlled at least in part by a NAM-like circulation response to orbital forcing. The raw time series of European SAT (light gray curve in Fig. 7) serves as a reminder that some warming could also be explained by internal NAM variability; the internal variability in the SAT time series—well correlated with the internal NAM—is comparable in magnitude to its orbital counterpart.

Figure 6b also shows that the Middle East experiences cold anomalies when the orbital NAM index is high. Our results are therefore also in harmony with the work of Felis et al. (2004), who found that Red Sea corals record colder wintertime temperatures during the Eemian period. As in our study, these authors find a high-NAM-index pattern dominating the wintertime temperature response of a climate model to Milankovitch forcing during the Eemian period, and infer from

this that the coral signals they uncover are likely driven by anomalies in the atmospheric circulation.

Finally, we note that several studies have identified NAM-like patterns dominating the NH wintertime atmosphere response to other types of external forcings, such as increasing greenhouse gases, volcanic forcing, and changes in solar irradiance (Robock and Mao 1995; Shindell et al. 1999; Fyfe et al. 1999; Shindell et al. 2001; Stenchikov et al. 2002; Gillett et al. 2002; Shindell et al. 2004). Therefore our study adds to the growing body of evidence that the NAM-like patterns are excited by external forcings with a wide variety of spatial structures and time scales.

Acknowledgments. Alex Hall is supported by NSF Grant ATM-0002833, A. Clement by NSF Grant ATM-0134742, and D. W. J. Thompson by NSF Grants ATM-0132190 and ATM-0320959. The authors wish to thank the Geophysical Fluid Dynamics Laboratory (Princeton, NJ) for making available the computational resources necessary to do this experiment. In addition, the authors wish to thank two anonymous reviewers, as well as Paul Kushner, for their constructive criticism of an early draft, leading to significant improvements in the final manuscript.

REFERENCES

Aalbersberg, G., and T. Litt, 1998: Multiproxy climate reconstructions for the Eemian and early Weichselian. *J. Quat. Sci.,* **13,** 367–390.

Berger, A., 1992: Orbital variations and insolation database. NOAA/NGDC contribution 92-007, NOAA/NGDC, Boulder, CO. [Available online at http://gcmd.nasa.gov/records/GCMD_EARTH_LAND_NGDC_PALEOCLIM_INSOL.html.]

Clement, A. C., R. Seager, and M. A. Cane, 1999: Orbital controls on the El Niño/Southern Oscillation and the tropical climate. *Paleoceanography,* **14,** 441–456.

Felis, T., G. Lohmann, H. Kuhnert, S. J. Lorenz, D. Scholz, J. Pätzold, S. A. Al-Rousan, and S. M. Al-Moghrabi, 2004: Increased seasonality in Middle East temperatures during the last interglacial period. *Nature,* **429,** 164–168.

Fyfe, J. C., G. J. Boer, and G. M. Flato, 1999: The Arctic and Antarctic Oscillations and their projected changes under global warming. *Geophys. Res. Lett.,* **26,** 1601–1604.

Gillett, N. P., M. R. Allen, R. E. McDonald, C. A. Senior, D. T. Shindell, and G. A. Schmidt, 2002: How linear is the Arctic Oscillation response to greenhouse gases? *J. Geophys. Res.,* **107,** 4022, doi: 10.1029/2001JD000589.

Hartmann, D. L., and F. Lo, 1998: Wave-driven zonal flow vacillation in the Southern Hemisphere. *J. Atmos. Sci.,* **55,** 1303–1315.

Hays, J. D., J. Imbrie, and N. J. Shackleton, 1976: Variations in the Earth's orbit: Pacemaker of the Ice Ages. *Science,* **194,** 1121–1132.

Hurrell, J. W., 1995: Decadal trends in the North Atlantic Oscillation: Regional temperatures and precipitation. *Science,* **269,** 676–679.

——, Y. Kushnir, M. Visbeck, and G. Ottersen, 2003: An overview of the North Atlantic Oscillation. *The North Atlantic Oscillation: Climate Significance and Environmental Impact*, *Geophys. Monogr.*, Vol. 134, Amer. Geophys. Union, 1–35.

Imbrie, J., and Coauthors, 1984: The orbital theory of Pleistocene climate: Support from a revised chronology of the marine d18O record. *Milankovitch and Climate, Part 1,* A.L. Berger et al., Eds., D. Riedel, 269–305.

Jackson, C., and A. J. Broccoli, 2003: Orbital forcing of Arctic climate: Mechanisms of climate response and implications for continental glaciation. *Climate Dyn.,* **21,** 539–557.

Karoly, D. J., 1990: The role of transient eddies in low-frequency zonal variations of the Southern Hemisphere circulation. *Tellus,* **42A,** 41–50.

Kidson, J. W., 1988: Indices of the Southern Hemisphere zonal wind. *J. Climate,* **1,** 183–194.

Klotz, S., J. Guiot, and V. Mosbrugger, 2003: Continental European Eemian and early Wurmian climate evolution: Comparing signals using different quantitative reconstruction approaches based on pollen. *Global Planet. Change,* **36,** 277–294.

Kushnir, Y., W. A. Robinson, I. Blade, N. M. J. Hall, S. Peng, and R. Sutton, 2002: Atmospheric GCM response to extratropical SST anomalies: Synthesis and evaluation. *J. Climate,* **15,** 2233–2256.

Limpasuvan, V., and D. L. Hartmann, 2000: Wave-maintained annular modes of climate variability. *J. Climate,* **13,** 4414–4429.

Lorenz, D. J., and D. L. Hartmann, 2003: Eddy-zonal flow feedback in the Northern Hemisphere winter. *J. Climate,* **16,** 1212–1227.

Philander, G. S., 1990: *El Niño, La Niña, and the Southern Oscillation*. Academic Press, 293 pp.

Robinson, W. A., 2000: A baroclinic mechanism for the eddy feedback on the zonal index. *J. Atmos. Sci.,* **57,** 415–422.

Robock, A., and J. Mao, 1995: The volcanic signal in surface temperature observations. *J. Climate,* **8,** 1086–1103.

Shindell, D. T., R. L. Miller, G. A. Schmidt, and L. Pandolfo, 1999: Simulation of recent northern winter climate trends by greenhouse-gas forcing. *Nature,* **399,** 452–455.

——, G. A. Schmidt, M. E. Mann, D. Rind, and A. Waple, 2001: Solar forcing of regional climate change during the Maunder Minimum. *Science,* **294,** 2149–2152.

——, ——, ——, and G. Faluvegi, 2004: Dynamic winter climate response to large tropical volcanic eruptions since 1600. *J. Geophys. Res.,* **109,** D05104, doi:10.1029/2003JD004151.

Stenchikov, G., A. Robock, V. Ramaswamy, M. D. Schwarzkopf, K. Hamilton, and S. Ramachandran, 2002: Arctic Oscillation response to the 1991 Mount Pinatubo eruption: Effects of volcanic aerosols and ozone depletion. *J. Geophys. Res.,* **107,** 4803, doi:10.1029/2002JD002090.

Thompson, D. W. J., and J. M. Wallace, 2000: Annular modes in the extratropical circulation. Part I: Month-to-month variability. *J. Climate,* **13,** 1000–1016.

Zagwijn, W. H., 1996: An analysis of Eemian climate in western and central Europe. *Quat. Sci. Rev.,* **15,** 451–469.